Communications Medicine

https://doi.org/10.1038/s43856-026-01477-x

Article in Press

Mapping neurophysiological biotypes of postpartum depression and underlying neural and molecular basis

Received: 24 June 2025

Accepted: 17 February 2026

Cite this article as: Chen, J., Liang, Y., Li, W. *et al.* Mapping neurophysiological biotypes of postpartum depression and underlying neural and molecular basis. *Commun Med* (2026). https://doi.org/10.1038/s43856-026-01477-x

Jin Chen, Ying Liang, Wei Li, Yashi Wu, Meiling Chen, Xingping Tao, Tiyan Zi, Xudong Dong, Bochao Cheng, Kexuan Chen & Jiaojian Wang

Mapping neurophysiological biotypes of postpartum depression and underlying neural and molecular basis

Short title: **PPD subtypes and molecular basis**

Jin Chen[1, 2, #], Ying Liang[1, 2, #], Wei Li[1, 2, #], Yashi Wu[1, 2], Meiling Chen[3], Xingping Tao[4], Tiyan Zi[5], Xudong Dong[6, *], Bochao Cheng[7, *], Kexuan Chen[8, *], Jiaojian Wang[1, 2, *]

[1]State Key Laboratory of Primate Biomedical Research, Institute of Primate Translational Medicine, Kunming University of Science and Technology, Kunming, China.

[2]Yunnan Key Laboratory of Primate Biomedical Research, Kunming, China.

[3]Department of Clinical Psychology, the First People's Hospital of Yunnan Province, The Affiliated Hospital of Kunming University of Science and Technology, Kunming, China.

[4]Department of Respiratory medicine, Children's Hospital, People's Hospital of Kaiyuan, Kaiyuan, China.

[5]Obstetrics Department, People's Hospital of Kaiyuan, Kaiyuan, China.

[6]Obstetrics Department, the First People's Hospital of Yunnan Province, The Affiliated Hospital of Kunming University of Science and Technology, Kunming, China.

[7]Department of Radiology, West China Second University Hospital of Sichuan University, Chengdu, China.

[8]Medical School, Kunming University of Science and Technology, Kunming, China.

#These authors contributed equally to this work

***Correspondence Address:**

[*]Correspondence: Jiaojian Wang, Kexuan Chen, Bochao Cheng and Xudong Dong

Email: jiaojianwang@uestc.edu.cn (J.W.), kexuanchen@kust.edu.cn (K.C.), wonder9527@163.com (B.C.), xudong52@outlook.com (X.D.)

Abstract

Background

Postpartum depression is a common and disabling condition that differs from major depressive disorder and shows marked variation in symptoms and outcomes. Identifying distinct biological subtypes could improve diagnosis and treatment. The present study aims to uncover neurophysiological subtypes of postpartum depression and explore their underlying neural and molecular features.

Methods

We analyzed structural brain images from a cohort of postpartum women recruited at the West China Second Hospital, Sichuan University, including 76 patients with postpartum depression and 62 healthy postpartum women (age range: 23-40 years). An unsupervised clustering approach was applied to gray matter volume patterns to identify neurobiological subtypes. Individualized structural covariance networks were then constructed to compare subtype-specific connectivity. Transcriptomic profiles and neurotransmitter density maps were further integrated to examine molecular mechanisms underlying the structural alterations.

Results

Here we show that postpartum depression can be divided into two neurobiological subtypes. Subtype 1 displays reduced gray matter volume in the dorsal attention network, consistent with cognitive impairments. Subtype 2 shows increased gray matter volume in the default mode network, reflecting emotional dysregulation. Subtype 2 also exhibits weaker structural connectivity between the middle temporal gyrus, parahippocampus, and amygdala. Molecular analysis indicates that Subtype 1 is related to energy metabolism and the neurotransmitter receptor $mGluR_5$, whereas Subtype 2 is associated with synaptic regulation, neuroplasticity, and neurotransmitter receptors such as $5\text{-}HT_{1B}$, dopamine D_2, cholinergic M_1 and μ-opioid receptor (MOR).

Conclusions

These findings suggest that postpartum depression comprises two biologically distinct forms with different cognitive and emotional characteristics. Recognizing these subtypes may enhance our understanding of its neuropathology and support the development of personalized therapeutic strategies.

Plain Language Summary

After childbirth, some women experience a serious form of depression called postpartum depression. This condition affects thinking, emotions, and daily life, but not all women experience it in the same way. In this study, we used brain scans to see if there are different types of postpartum depression based on brain structure. We found two groups: one showing changes in brain areas linked to attention and thinking, and another showing changes in regions involved in emotions. These differences were also reflected in brain chemistry and gene activity. Our findings suggest that postpartum depression is not one single disorder, and understanding its biological types may help doctors offer more personalized care and treatment in the future.

Introduction

Postpartum depression (PPD) is a common mental disorder among women during the perinatal period, characterized by obvious mood swings, loss of interest, and sleep disturbances, which can seriously affect the mother-child relationship, child development, and family stability[1,2]. Traditionally, the PPD is considered to be a subtype of general depression occurring outside the perinatal period, but emerging evidence suggests that PPD is different from general depression[3-6]. Although PPD is diagnosed using the same criteria, PPD exhibits significant heterogeneity in clinical manifestations, symptom severity, and treatment response, which suggests that PPD may have different neurophysiological subtypes[7-9]. However, almost all the previous studies regarded PPD as a homogeneous disorder ignoring the neuropathological complexity[10-12]. Therefore, identifying neurophysiological subtypes of PPD using objective neuroimaging biomarkers could facilitate our understanding of different neurobiological mechanisms underlying the clinical heterogeneity of PPD and ultimately improve both diagnosis and treatment.

With the development of magnetic resonance imaging (MRI) technology and computational neuroscience, an increasing number of studies have begun to identify biological subtypes of brain diseases based on non-invasive neuroimaging features[13-15]. Compared with traditional disease classification using clinical scales or symptoms, neuroimaging-based brain disorders subtyping can better uncover the underlying neurobiological mechanisms of the heterogeneity of diseases and contributes to the development of precision treatment[16]. Compared with functional and diffusion MRI, structural MRI has many advantages such as easy access, high signal-to-noise ratio and test-retest reproducibility[17,18]. Structural MRI as well as its derived measure of gray matter volume (GMV) which is an important indicator reflecting neural development, plasticity, and long-term stress adaptation has been widely used to explore the structural abnormalities of PPD[19-21]. Given that the coordinated changes in brain structures of spatially different regions are fundamental to functional development, structural covariance network (SCN) is developed[18,22,23]. In early studies, the SCN is constructed at the group-level[24,25]. Given that the group-level SCN is hard to reflect the individual variations and relationships with behaviors, the individual differential structural covariance network (IDSCN) was proposed to reveal the abnormal covariance connectivity in brain disorders[26-29].

In this study, we use spectral clustering based on GMV derived from structural MRI to define biological subtypes of PPD and to identify subtype-specific structural abnormal patterns. Moreover, we further apply IDSCN approach to reveal the differences in structural covariance connectivity between PPD subtypes. Finally, by integrating transcriptomic data from the Allen Human Brain Atlas (AHBA) with neurotransmitter density maps, a methodology widely used in neuroimaging studies[30], we establish the molecular basis underlying the structural abnormalities of PPD subtypes.

Methods

Participants

Data for this study were derived from a longitudinal investigation of postpartum depression (PPD) conducted in Chengdu, China. All 138 postpartum women were screened and recruited at the Maternity Clinic, West China Second University Hospital of Sichuan University. Clinical diagnoses were conducted by two experienced psychiatrists from the same institution, adhering to the criteria outlined in the Diagnostic and Statistical Manual of Mental Disorders, Fifth Edition (DSM-5) and the Chinese Classification of Mental Disorders, Third Edition (CCMD-3). The recruitment period for the study ran from 1 June 2018 to 1 January 2020, with all participants being within one year postpartum (mean ± standard deviation = 96.54 ± 56.42 days). The sample included 62 healthy postpartum women (HPW) and 76 unmedicated patients with PPD. Exclusion criteria included cardiovascular disease, diabetes, other psychiatric disorders, suicide risk, a history of alcohol or substance abuse, contraindications to MRI, or evidence of intracranial pathology. Inclusion criteria were full-term delivery, normal puerperium, healthy newborn, right-handedness. All PPD patients were first-episode and drug-naive. All participants underwent the following assessments during the same research visit: (1) psychiatric evaluation; (2) serum hormone tests, including prolactin, estradiol, and progesterone; and (3) magnetic resonance imaging (MRI) scanning. This study was conducted in accordance with the Declaration of Helsinki and was approved by the Ethics Committee of West China Second Hospital, Sichuan University (No. S201731). Written informed consent was obtained from all participants prior to participation.

Clinical Assessments

Demographic and lifestyle information was collected for each participant, including age, postpartum days and educational level. Psychological and social variables were assessed using a battery of validated standardized questionnaires. Depressive symptoms were evaluated using the Edinburgh Postnatal Depression Scale (EPDS)[31] and the Beck Depression Inventory (BDI)[32], while anxiety levels were assessed using the Beck Anxiety Inventory (BAI)[33]. These instruments have demonstrated good reliability and validity in Chinese women of reproductive age. Sleep quality was measured using the Pittsburgh Sleep Quality Index (PSQI)[34], which captures various domains such as subjective sleep quality, sleep latency, duration, and daytime functioning. Postpartum social support was assessed using the Postpartum Support Questionnaire (PSQ)[35], which measures perceived emotional and instrumental support after childbirth. Perceived stress was evaluated using the Perceived Stress Scale (PSS)[36], a widely used instrument that captures subjective appraisal for individuals of stress over recent weeks. All assessments were conducted by trained evaluators with backgrounds in psychology or medicine, using either structured interviews or self-report questionnaires to ensure consistency and standardization of data collection.

Structural MRI Data Acquisition

All MRI data were acquired at West China Second University Hospital, Sichuan University, using a 3.0 MRI scanner (MAGNETOM Skyra, Siemens Healthcare, Erlangen, Germany). To minimize motion artifacts, participants' heads were stabilized using foam padding, with the head positioned centrally within the coil to ensure consistency and image quality. High-resolution anatomical images of the brain were obtained using a three-dimensional T1-weighted Magnetization Prepared Rapid Gradient Echo (T1-MPRAGE) sequence. The imaging parameters were as follows: repetition time (TR) = 3500ms, echo time (TE) = 2.29ms, flip angle = 8°, field of view (FOV) = 240 × 240, acquisition matrix = 256 × 256, voxel resolution = 0.9 × 0.9 × 1mm³.

Structural MRI Data Preprocessing

Voxel based morphometry (VBM) analysis was conducted using MATLAB 2021b and Statistical Parametric Mapping software (SPM8, http://www.fil.ion.ucl.ac.uk). First, all raw T1-weighted structural images were converted to NIFTI format. Using the unified segmentation module in SPM8 with default tissue probability maps (TPMs), images were normalized to the Montreal Neurological Institute (MNI152) standard space and segmented into gray matter, white matter, and cerebrospinal fluid. All segmentation and normalization results were visually inspected for quality assurance. Next, a study-specific gray matter template was generated using Diffeomorphic Anatomical Registration Through Exponentiated Lie algebra (DARTEL)[37]. This template was affine-registered to the standard MNI gray matter probability map to improve spatial normalization accuracy. Individual gray matter images were then warped to MNI space using the DARTEL nonlinear deformation fields and modulated to preserve the original tissue volumes. Finally, the normalized and modulated gray matter images were smoothed using an isotropic Gaussian kernel with a full width at half maximum (FWHM) of 6 mm to enhance signal-to-noise ratio and meet the assumptions of random field theory. The preprocessed gray matter images of each participant were used for subsequent analyses.

Statistics and Reproducibility

Define the PPD Subtypes Using Spectral Clustering. Spectral clustering with the whole brain GMV as features was applied to define subtypes of PPD. First, a symmetric similarity matrix W of size $n \times n$ was constructed by calculating the Pearson correlation coefficient between every pair of subjects, where $W_{(i.j)}$ represents the correlation of gray matter volume between subjects i and j, serving as the adjacency matrix. Next, the degree matrix D was formed as a diagonal matrix with diagonal elements $D_{(i.i)}$ equal to the sum of the corresponding row in W, representing the total connection strength of subject i, while off-diagonal elements were zero.

The unnormalized graph Laplacian matrix L was then computed as $L = D - W$. Subsequently, the symmetric normalized Laplacian matrix L_{sym} was calculated by

$$L_{sym} = D^{-1/2} L D^{-1/2}$$

The eigenvalues and corresponding eigenvectors of L_{sym} were computed and sorted in ascending order. The

first k smallest nonzero eigenvectors of eigenvalues were selected to form the feature matrix U. Each row of U was then normalized to have unit length, projecting the data onto a unit hypersphere. Finally, k-means clustering was performed on the normalized matrix U. The optimal number of clusters k was determined by evaluating silhouette coefficients across different number of clusters.

Specific GMV Abnormal Patterns of PPD Subtypes. To identify specific GMV abnormal patterns for PPD subtypes, two-sample t-tests were used to identify GMV differences for each subtype of PPD compared to HPW. The significances of these statistical analyses were determined using Gaussian Random Field (GRF) correction with $p < 0.05$.

Functional Decoding for Subtype-specific GMV Difference Maps. To determine the main functions of brain regions showing significant GMV difference of each PPD subtype compared to HPW, we performed functional decoding using a Neurosynth meta-analysis. Meta-analytic decoding was conducted using 24 topic terms defined by Margulies et al[38]. The analysis yielded z-statistic values indicating the strength of association between each brain region and topic term. Terms with z-statistics greater than 3.1 (corresponding to $p < 0.05$, false discovery rate (FDR)-corrected) were considered significantly associated.

Individualized Structural Covariance Network Analysis for PPD Subtypes. The structural covariance network for healthy controls was constructed using the individual structural covariance network (IDSCN) method described by Liu et al.[39]. The voxel-wise GMV maps of each participant were parcellated into 116 regions using the Automated Anatomical Labeling (AAL) atlas. For each participant, the mean GMV value of all voxels within each region was calculated, resulting in 116 regional GMV measures per participant. The structural covariance network for healthy controls was generated by calculating the Pearson correlation coefficient between every pair of brain regions across all healthy controls, serving as the reference network PCC_n. Each PPD patient from the subtypes was added to the healthy control group, and a new structural covariance network PCC_{n+1} was computed, forming the perturbed network. The difference between the perturbed and reference networks, $\Delta\mathrm{PCC}_n = \mathrm{PCC}_{n+1} - \mathrm{PCC}_n$ represented the IDSCN for each patient, reflecting changes in covariance between brain regions relative to the healthy baseline. The z-scores of $\Delta\mathrm{PCC}_n$ were calculated using

$$\Delta\mathrm{PCC}_{n_z} = \frac{\Delta\mathrm{PCC}_n}{\frac{1-\mathrm{PCC}_n^2}{n-1}}$$

For each participant, z-scores were calculated for all network edges relative to the healthy control distribution. These z-scores were converted into two-tailed *p*-values. To control for multiple comparisons across edges within each participant, FDR correction (Benjamini-Hochberg method) was applied across all edges for that participant. Subsequently, for each edge, we counted the number of participants whose FDR-corrected *p*-value was below 0.05.

This count represents how consistently a given edge showed significant alteration across participants (e.g., significant in ≥10% of patients).

Transcriptomic Association Analyses for GMV Difference of Each PPD Subtype. The Allen Human Brain Atlas dataset (https://human.brain-map.org/) was used to explore the relationship between whole-brain t-maps of PPD subtypes compared with HPW and genes' expression profiles[40]. Gene's expression data were obtained from six postmortem adult human brains. According to the dataset description, these donors consisted of both male and female individuals without documented psychiatric diagnoses. Microarray expression data were preprocessed using the abagen toolbox[41], which implements a reproducible workflow based on a well-established processing protocol[42]. After preprocessing with the Schaefer atlas (500 parcels)[43], a regional gene expression matrix was generated for each donor, comprising 500 rows (brain regions) and 15,633 columns (genes). Because of sampling bias and only two samples have the samples in right hemisphere, thus, in this study, we only used the transcriptomic data of the left hemisphere, we finally obtained a 250 × 15,633 matrix representing. Partial least squares (PLS) correlation analysis was conducted to assess the relationship between regional t-values (derived from comparisons between PPD subtype and HPW) and the expression profiles of 15,633 genes. The whole-brain t-map was resampled to match the 500-region parcellation by averaging voxel values within each parcel. In the PLS analysis, gene expression profiles were treated as the predictor matrix, and the t-values were used as the response vector. The first PLS component (PLS1) showed a strong spatial correlation with the t-map across the 250 regions. To estimate the contribution of each gene to PLS1, a bootstrap procedure (1,000 iterations) was applied to compute standard errors of gene weights. z-scores were calculated by dividing the gene weights by their bootstrap-derived standard errors, and genes were then ranked based on their z-scores, reflecting their relative contribution to PLS1.

Neurotransmitter Receptors and Transporters Association Analysis. To identify neurotransmitters associated with the GMV differences of each PPD subtype, we examined the spatial relationships between the whole-brain t-maps (each PPD subtype compared to HPW) and the spatial distributions of neurotransmitter systems. The whole-brain volumetric PET receptor/transporter maps were obtained from a publicly available dataset (https://github.com/netneurolab/hansen_receptors/tree/main/data/PET_nifti_images)[44], which comprises data from a large sample of over 1,200 healthy individuals. This cohort includes both male and female participants. It is important to note that these PET data were derived from an independent cohort of healthy volunteers, distinct from the participants in our present study. The 19 distinct neurotransmitter maps were assigned to 500 regions, and the averaged value of all voxels within the region was defined as the region's neurotransmitter value. After normalizing each neurotransmitter map across 500 regions, we used a multivariate linear regression model to explore the contributions of neurotransmitter systems to the GMV difference. From this model, we extracted the *p*-values corresponding to each neurotransmitter. To correct for multiple comparisons, we applied FDR correction at a threshold of $p < 0.05$.

Results

Participants and Demographic Characteristics

A total of 138 participants, including 62 HPW and 76 women with postpartum depression (PPD), were included in the study. As shown in Table 1, no significant group differences were observed in postpartum time (p = 0.96), hormonal measures including estradiol, progesterone, and prolactin (p = 0.59, p = 0.80, and p = 0.77), or education level (p = 0.68). Although age showed a modest group difference (t = -2.108, p = 0.04, Cohen's d = -0.37), the effect size was small. In contrast, participants with PPD showed significantly higher scores in all clinical measures, including the Edinburgh Postnatal Depression Scale (EPDS; t = 13.95, p < 0.001, d = 2.37), Beck Anxiety Inventory (BAI; t = 8.27, p < 0.001, d = 1.34), Beck Depression Inventory (BDI; t = 10.27, p < 0.001, d = 1.63), Pittsburgh Sleep Quality Index (PSQI; t = 4.99, p < 0.001, d = 0.85), and Perceived Stress Scale (PSS; t = 5.69, p < 0.001, d = 0.98), indicating that the depression, anxiety, sleep quality, and perceived stress are abnormal in PPD. Detailed demographic and clinical characteristics are presented in Table 1.

Table 1. Demographics and Clinical Characteristics of the Subjects Used in Present Study

	PPD (n=76)	HPW (n=62)	t-value	Cohen's d	PPD vs HPW
Age (years)	31.08 ± 3.44	32.42 ± 3.92	-2.11	-0.37	p = 0.037
Education (years)	16.62 ± 1.77	16.50 ± 1.61	0.41	0.07	p = 0.682
Postpartum time (days)	96.76 ± 54.75	96.27 ± 58.86	0.05	0.01	p = 0.960
Estradiol (pg/ml)	52.84±185.89	81.23±372.80	-0.55	-0.10	p = 0.586
Progesterone (ng/ml)	0.88±2.36	0.79±1.41	0.25	0.04	p = 0.800
Prolactin (ng/ml)	81.04±64.75	77.66±67.39	0.30	0.05	p = 0.766
EPDS scores	17.29 ± 4.45	7.06 ± 4.14	13.95	2.37	p < 0.001
BAI	43.92 ± 11.38	30.73 ± 7.23	8.27	1.36	p < 0.001
BDI	20.20 ± 9.01	7.24 ± 5.70	10.27	1.68	p < 0.001
PSQI	9.87 ± 3.67	6.85 ± 3.41	4.99	0.85	p < 0.001
PSS	20.05 ± 4.52	15.50 ± 4.80	5.69	0.98	p < 0.001

Two-sample t-test is used (two-sided) to determine the between-group differences. PPD: postpartum depression; HPW: healthy postpartum women; EPDS: Edinburgh Postnatal Depression Scale; BAI: Beck Anxiety Inventory; BDI: Beck Depression Inventory; PSQI: Pittsburgh Sleep Quality Index; PSS: Perceived Stress Scale.

Define PPD Subtypes and Their Specific Structural Abnormal Patterns

To define the neurophysiological subtypes of PPD, we performed clustering analysis based on the whole-brain GMV using a spectral clustering algorithm. The optimal number of clusters was determined using the silhouette coefficient across different cluster numbers. The silhouette coefficient peaked at two clusters (coefficient = 0.69,

Figure 1a), indicating the most robust clustering solution. Based on the clustering result, PPD patients were divided into two neurophysiological subtypes: Subtype 1 (n = 44) and Subtype 2 (n = 32). Table 2 summarizes the demographic, hormonal, and clinical characteristics across HPW (n = 62), Subtype 1, and Subtype 2, as well as their pairwise comparisons. Compared to HPW, both Subtype 1 and Subtype 2 showed significantly higher scores on the EPDS, BAI, BDI, PSQI, and PSS (all $p < 0.05$). Subtype 2 exhibited slightly higher BAI and PSS scores than Subtype 1, suggesting a tendency toward greater anxiety and stress perception. In addition, no significant group differences were observed in education or postpartum time, while age showed a modest decrease in Subtype 2 compared to HPW (p = 0.016). For hormonal measures, we observed a marginal difference in progesterone between PPD subtypes (p = 0.140) with the subtype 1 showing lower progesterone compared with subtype 2. The other two hormonal measures of estradiol and prolactin did not show significant group differences. Overall, these results indicate that both PPD subtypes exhibit elevated depressive, anxiety, sleep, and stress symptoms relative to healthy postpartum women, with Subtype 2 showing comparatively greater emotional dysregulation.

Table 2. Demographics, Hormonal Levels, and Clinical Characteristics of HPW and Subtypes

	HPW (*n*=62)	**Subtype 1 (*n*=44)**	**Subtype 2 (*n*=32)**	**HPW vs Subtype 1**	**HPW vs Subtype 2**	**Subtype 1 vs Subtype 2**
Age(years)	32.42±3.92	31.59 ± 3.22	30.38 ±3.67	p = 0.252	p =0.016	p = 0.129
Education (years)	16.50±1.61	16.89± 1.81	16.25 ±1.68	p = 0.250	p =0.484	p = 0.123
Postpartum time (days)	96.27±58.86	93.14±52.43	101.75±58.27	p = 0.778	p =0.669	p = 0.502
Estradiol (pg/ml)	81.23±372.80	35.88±28.74	76.17±285.46	p = 0.423	p =0.947	p = 0.354
Progesterone (ng/ml)	0.79±1.41	0.47±0.22	1.43±3.58	p = 0.081	p =0.339	p = 0.140
Prolactin (ng/ml)	77.66±67.39	84.43±69.84	76.38±57.78	p = 0.617	p =0.927	p = 0.596
EPDS scores	7.06 ± 4.14	17.75± 3.81	16.66 ± 5.20	p = 0.001	p < 0.001	p = 0.293
BAI	30.73± 7.23	42.20 ± 9.62	46.28±13.22	p = 0.001	p < 0.001	p = 0.124
BDI	7.24 ± 5.70	20.86 ± 8.84	19.28± 9.30	p = 0.001	p < 0.001	p = 0.453

PSQI	6.85± 3.41	9.93± 3.97	9.78 ± 3.26	$p = 0.001$	$p < 0.001$	$p = 0.861$
PSS	15.50 ± 4.80	19.73±4.05	20.50±5.14	$p = 0.001$	$p < 0.001$	$p = 0.466$

Two-sample *t*-test (two-sided) is used to determine the between-group differences. PPD: postpartum depression; HPW: healthy postpartum women; EPDS: Edinburgh Postnatal Depression Scale; BAI: Beck Anxiety Inventory; BDI: Beck Depression Inventory; PSQI: Pittsburgh Sleep Quality Index; PSS: Perceived Stress Scale.

Whole-brain voxel-level GMV analysis revealed significant differences between the two PPD subtypes compared with HPW. Subtype 1 showed significant reductions of GMV primarily in the superior parietal lobule/precuneus and inferior parietal lobes which are mainly localized in the dorsal attention network (DOR) and a part of somatosensory motor network (SOM) (Figure 1b). Functional decoding indicated that these regions are involved in action, motor control, pain, and spatial processing. In contrast, Subtype 2 showed increased GMV predominantly in the posterior cingulate cortex (PCC) (Figure 1c). The PCC is a core hub of the default mode network (DMN), implicated in social cognition, emotion processing, recollection, and autobiographical memory. When directly comparing the two PPD subtypes, Subtype 1 exhibited significantly lower GMV than Subtype 2 mainly in the bilateral parietal and occipital cortices, including the precuneus, superior parietal lobule, and lateral occipital areas (Figure 1d). These regions were largely distributed within the ventral attention network (VEN), with some involvement of the visual (VIS) networks.

In addition, we examined voxel-wise correlations between whole-brain GMV and both depressive symptom severity and reproductive hormone levels separately in Subtype 1 ($n = 44$) and Subtype 2 ($n = 32$) (Figure 1e). We further assessed, for each subtype, the mean GMV extracted from the regions that showed significant differences relative to healthy postpartum women (HPW). As shown in Figure 1f, the mean GMV of Subtype 1 displayed a potentially significant negative association with EPDS ($r = -0.39$, $p\_uncorrected < 0.05$) and BDI scores ($r = -0.31$, $p\_uncorrected < 0.05$), indicating that smaller GMV in these attention- and cognition-related regions was associated with more severe depressive symptoms. Subtype 1 GMV also showed a potentially significant negative correlation with prolactin levels ($r = -0.22$, $p\_uncorrected < 0.05$). For Subtype 2, the mean GMV extracted from regions showing potentially significant differences relative to HPW was also negatively correlated with prolactin levels ($r = -0.17$, $p\_uncorrected < 0.05$). Correlations with estradiol and progesterone were weak and did not reach significance for either subtype. We also examined the regions showing potentially significant GMV differences between Subtype 1 and Subtype 2 and found that their mean GMV was negatively associated with EPDS scores ($r = -0.19$, $p\_uncorrected < 0.05$). Together, these results suggest that both depressive severity and prolactin levels may be related to the structural alterations defining Subtype 1, whereas prolactin levels may also be related to the regional GMV reductions characteristic of Subtype 2.

The IDSCN Differences between PPD Subtypes

To investigate individualized structural covariance connectivity abnormalities in PPD subtypes, we constructed an individual-level structural covariance network (IDSCN) for each participant using the AAL atlas, resulting in a total of 6,670 structural covariance connections. By comparing these connections with those of healthy postpartum women (HPW), 6,040 edges showed significant deviations in at least one PPD patient, and 4,564 edges were shared by at least two individuals, suggesting a certain degree of consistency in network alteration patterns among PPD patients (z-values across all patients was 0.06 ± 0.17). The number of significantly deviating connections per patient ranged from 0 to 2,108 (0%–31.6% of all edges), with an average of 207.76 ± 373.84, indicating high heterogeneity in structural covariance changes between individuals ($p < 0.05$, FDR-corrected). To identify the most consistently affected connections, we further extracted 26 edges that showed significant deviations in at least 8 individuals (>10%). These edges primarily involved regions such as the middle temporal gyrus (MTG), amygdala (AMYG), and para hippocampal gyrus (PHG) (Figures 2a and 2b).

Further comparison of the z-values for these 26 edges between PPD subtypes revealed some significant differences between the two subtypes. Subtype 2 exhibited significantly lower structural covariance connections between left MTG (MTG.L)-left PHG (PHG.L) and between right MTG (MTG.R)-right AMYG (AMYG.R) compared with Subtype 1 (Figure 2c, $p < 0.001$, FDR corrected).

Transcriptomic Correlates of Structural Alterations of PPD Subtypes

We employed partial least squares (PLS) regression to assess the spatial association between regional gene expression profiles and subtype-specific structural alterations (group-level t-maps) in PPD. Our analyses focused on the first two components (PLS1 and PLS2), where PLS1 captured the largest portion of spatial variance in cortical gene expression (explaining 16% of variance in Subtype 1 and 14% in Subtype 2). Both PLS1 and PLS2 scores were significantly positively correlated with the subtype-specific t-maps ($r_1 = 0.40$, $p < 0.05$; $r_2 = 0.33$, $p < 0.05$; Figures 3a and 3b).

To screen for the most significant genes, we ranked the PLS1 weights using a one-sample z-test. In Subtype 1, we identified 5762 genes with significant positive or negative weights ($|z| > 2.35$, FDR-corrected $p < 0.05$) associated with the group-level structural alterations. In Subtype 2, 3875 such genes were identified ($|z| > 2.40$, FDR-corrected $p < 0.05$). These gene sets were subjected to Gene Ontology (GO) enrichment analysis to uncover biological processes and molecular functions relevant to regional brain abnormalities in each subtype.

For Subtype 1, the top five enriched biological processes (BP) and molecular functions (MF) were predominantly related to mitochondrial energy metabolism, redox processes, and ubiquitin-mediated proteolysis. These included aerobic respiration, cellular respiration, and proteasome-mediated ubiquitin-dependent protein catabolic processes (BP), as well as ubiquitin protein ligase binding and ribonucleoprotein complex binding (MF) (Figure 3a). In contrast, the gene set associated with Subtype 2 was enriched in pathways related to

neurodevelopment and synaptic function. The top BPs included axonogenesis, synapse organization, and regulation of cell component size, while the top MFs were metal ion transmembrane transporter activity, GTPase regulator activity, and voltage-gated sodium channel activity (Figure 3b).

Neurotransmitter Correlates of Structural Alterations in PPD Subtypes

We further explored the spatial correlation between group-level t-maps and neurotransmitter receptor density maps. In Subtype 1, regional structural alterations were significantly negatively correlated with the distribution of $mGluR_5$ receptors (r = -0.50; Figure 4). In Subtype 2, structural changes were negatively associated with the distribution patterns of $5\text{-}HT_{1B}$ (r = -0.31) and D_2 (r = -0.29) receptors but positively associated with M_1 (r = 0.31) and MOR (μ-opioid receptor; r = 0.32) density maps (Figure 4).

Discussion

This study identifies two distinct neurobiological subtypes of PPD using an unsupervised clustering algorithm based on GMV. Specifically, Subtype 1 is characterized by reduced GMV in the DOR, while Subtype 2 is characterized by increased GMV in the default mode network (DMN). The different structural abnormal patterns of PPD subtypes indicate that PPD has two different subtypes: cognitive impairment and emotion dysregulation. This interpretation aligns with recent stratification work in perinatal depression, such as the study by Bauer et al.[45], which demonstrated the value of data-driven subtyping for capturing clinically meaningful heterogeneity. Further analyses, including individualized structural covariance networks (IDSCN), transcriptomic mapping, and neurotransmitter density profiles, revealed distinct connectivity and molecular signatures for each subtype. Together, these results indicate that the clinical heterogeneity of PPD is supported by divergent neurophysiological mechanisms, reinforcing the need for stratified approaches in perinatal mental health research.

Subtype 1 primarily exhibited a reduction in GMV in regions including the superior parietal lobe/precuneus and inferior parietal lobule, which are primarily involved in DOR. The DOR is associated with goal-directed attention control, sensorimotor integration, and monitoring of the external environment in mothers, and plays an important role in PPD[46,47], The reduction in grey matter volume in this region may lead to cognitive impairments in patients, such as decreased attention span and difficulty in task regulation[48]. This is consistent with the clinical symptoms of significant cognitive decline in some PPD patients[49,50]. IDSCN analysis further revealed enhanced connectivity between MTG and AMYG, PHG in Subtype 1, suggesting that non-adaptive compensation may occur in emotion processing-related pathways, i.e., maintaining relative stability of overall function by enhancing regional connectivity. However, this excessive connectivity may not be an effective compensation but may instead lead to a weakening of the patient's ability to control attention. The existing researches have shown that excessive strengthening of the connection between the middle temporal gyrus and the limbic system may be related to a decline in an individual's ability to selectively process emotional or cognitive information[51,52]. This differs from MDD, where extensive research has found that functional connectivity between the amygdala and the temporal lobe and par hippocampal gyrus is disrupted in MDD[53-55]. In terms of clinical phenotype, although the EPDS score for this subtype is relatively high, the BAI score and PSS stress score are relatively low, and it is more likely to manifest as postpartum depression-like symptoms centered on cognitive fatigue and lack of attention[1,56]. At the same time, this subtype scored lower on the PSQI sleep quality scale, suggesting that its cognitive regulation disorders may interact with sleep rhythm disturbances and cognitive impairment to jointly constitute the PPD neurophenotype, which is characterized by cognitive fatigue and attention deficit[56,57]. Transcriptome analysis further revealed that Subtype 1 exhibits distinct features such as mitochondrial energy metabolism disorders, elevated oxidative stress levels, and protein homeostasis imbalances. These changes may constitute the underlying pathological mechanisms of PPD structural damage[58,59]. The density of the glutamate receptor mGluR5 shows a significant negative correlation with structural disturbances in Subtype 1, suggesting that the glutamate system may be impaired, leading

to restricted excitatory transmission function in neurons. It is suggested that impaired glutamatergic transmission in PPD patients may limit synaptic plasticity and neural integration capacity, further exacerbating cognitive decline[60,61]. In summary, Subtype 1 can be classified as a PPD neurobiological Subtype characterized by cognitive impairment accompanied by attention deficits and sleep disorders, driven by neuroenergetic metabolic disorders and glutamatergic system dysfunction. Future treatments should consider targeting neural energy metabolism, enhancing cognitive regulation capacity, and improving sleep structure to achieve targeted interventions[62-64].

In contrast to Subtype 1, Subtype 2 showed increased GMV in the PCC, which serve as core nodes of DMN[65,66], and plays important roles in emotional regulation, self-referential processing, and introspective thinking[47,67,68]. The DMN has been shown to be involved in regulating postpartum depression levels, and abnormal activation of the DMN is closely related to increased negative emotions and emotional regulation difficulties in PPD patients[1,69]. The increased GMV of PCC in PPD patients may be due to prolonged hyperactivity in these regions, leading to structural plasticity changes that exacerbate emotional regulation difficulties and negative emotional experiences, which is consistent with a previous research's findings[70]. The IDSCN results for this Subtype showed significantly weakened connections between MTG and AMYG, PHG, which are brain regions that collectively participate in emotion recognition, memory integration, and response regulation[11,71-73], These damaged connections indicate that PPD patients have reduced information integration capabilities in their emotional processing pathways, leading to more pronounced emotional regulation disorders, including emotional fluctuations, cognitive biases, and persistent rumination[5,74]. Accordingly, this subtype scored numerically higher on the BAI and the PSS Stress Scale than Subtype 1, suggesting that it exhibits stronger stress perception and emotional arousal responses. Combined with its significant DMN structural alterations and network characteristics, this subtype may correspond to individuals with higher stress loads, suggesting a higher risk of chronicity and weakened emotional regulation abilities. At the molecular level, Subtype 2 showed significant abnormalities in neural development and synaptic plasticity pathways, further supporting the association between emotional regulation disorders and structural plasticity changes in this group of patients[75]. Neurotransmitter analysis results showed that the structural abnormalities of this subtype were negatively correlated with 5-HT_{1B} and D_2 receptor density, while positively correlated with M_1-type cholinergic receptor and μ-opioid receptor density, suggesting an imbalance in the regulation between multiple neurotransmitter systems[47]. In PPD patients, the reduced density of 5-HT_{1B} and D_2 receptors suggests that this subtype may be associated with down-regulation of serotonin and dopamine system function, which is closely related to decreased emotional inhibition and blunted reward response[1,76]. Consistent with findings in MDD, excessive engagement of the DMN during rest enhances rumination, thereby exacerbating depressive mood[77]. Concurrently, increased densities of M_1 cholinergic receptors and μ-opioid receptors in this subtype may heighten patients' sensitivity to endogenous pain and emotional stimuli, inducing more intense emotional fluctuations and negative experiences[78,79]. This differs from the monoamine deficiency observed in MDD[80]. The imbalance between the aforementioned multi-pathway neurotransmitter systems may jointly drive abnormal structural and functional

changes in DMN-related brain regions, further disrupting emotional regulation and self-processing mechanisms, thereby making PPD patients more prone to recurrent negative introspection and emotional distress[81,82]. In summary, the neural structure and molecular characteristics of this subtype collectively contribute to a postpartum depression neural phenotype characterized by dysregulation of emotional control. Future treatment strategies should focus on cognitive behavioural therapy centered on emotional restructuring, or rTMS neuromodulation targeting the PCC, which may help alleviate emotional regulation disorders in patients with this subtype.

When directly comparing the two PPD subtypes, Subtype 1 exhibited significantly lower gray matter volume in the bilateral parietal and occipital cortices compared to Subtype 2. These regions are primarily distributed within the VEN and VIS, and are mainly involved in motor control, visual-spatial processing, and visual attention. This indicates that compared to Subtype 2, Subtype 1 exhibits more pronounced structural deficits in attention and perception-related systems, while Subtype 2 demonstrates relatively intact or compensatory enlargement in these regions. This aligns with the previously described clinical differences between cognitive and affective subtypes. Notably, these anatomical differences carry clinical and endocrinological significance. The mean gray matter volume in Subtype 1 specific regions negatively correlated with depression severity (EPDS score) and prolactin levels. These findings suggest that reduced gray matter volume in the parietal and occipital lobes of Subtype 1 patients correlates with increased symptom burden, and that prolactin dysregulation may be associated with decreased gray matter volume within the attention perception network. The mechanism may involve stress modulating neuroplasticity in these regions via lactation related prolactin signaling pathways, thereby exacerbating cognitive fatigue and attentional control phenotypes in Subtype 1 patients[83,84]. Conversely, the relative anatomical integrity of visual-frontal and visual-temporal networks in Subtype 2 patients aligns with their emotional and stress related characteristics.

Although this study revealed the neuroanatomical heterogeneity of PPD through individualized structural covariance networks and spectral clustering methods and linked subtype differences to molecular and neurotransmitter profiles, several limitations should be acknowledged. First, the sample size was modest, which may limit statistical power and generalizability. Future multi-center studies with larger cohorts are needed to verify the robustness and reproducibility of these subtypes. Second, the cross-sectional design precludes inference about longitudinal trajectories of these subtypes, such as persistence over time, treatment response, or prognostic implications, which limits direct translational applications. Third, the current analysis focused solely on structural MRI data. Integrating multimodal imaging such as functional or diffusion MRI and biological measures would provide a more comprehensive understanding of the neurophysiological mechanisms underlying PPD heterogeneity, and in the current study, we did not include direct cognitive performance measures such as attention or executive function test, the absence of direct cognitive assessment limits our ability to confirm whether cognitive deficits are indeed present in Subtype 1. Fourth, for the transcriptomic and neurotransmitter association analyses, both the Allen Human Brain Atlas and normative neurotransmitter atlases were based on mixed-sex healthy adult samples

independent of our cohort. While these normative datasets provide robust population-level molecular baselines for spatial comparison with our MRI maps and are consistent with prior neuroimaging transcriptomic studies, sex-related and clinical factors may influence gene expression and receptor distributions. Future work using sex-balanced and clinically stratified transcriptomic and neurochemical datasets will be necessary to refine these molecular associations and validate their specificity to PPD.

In conclusion, this study utilized structural MRI data to identify two neurobiological PPD subtypes through spectral clustering methods. Subtype 1 was characterized by specific structural damage in DOR while Subtype 2 has significant increased GMV in DMN. In addition, the two PPD subtypes showed significant differences in structural covariance connectivities of MTG with AMYG and PHG. The specific GMV and structural covariance connectivity differences indicated that PPD has two different subtypes: one is cognitive impairment and the other is emotion dysregulation. Moreover, the structural abnormal patterns of different PPD subtypes were regulated by different genes and neurotransmitters suggesting the different neuropathology underlying clinical heterogeneity of PPD. These findings provide initial evidence for different subtypes of PPD and identify the therapy targets for different subtypes, which will facilitate future precision diagnosis and treatment.

Data availability

Source data underlying the analyses presented in Figures 1-4 are available in Supplementary Data Sheets 1-4. The dataset analyzed in this study is available by requiring to the corresponding authors.

Acknowledgement

This study was supported by Yunnan Fundamental Research Projects (202501AV070005), National Natural Science Foundation of China (32560206), Yunnan Provincial International Joint R&D Center for Precision Healthcare in Maternal-Fetal Medicine (202503AP140051), Key Research and Development Plan of Yunnan Province (202403AC100002), Sichuan Science and Technology Program (2024TFFK0361), Natural Science Foundation of Chongqing (CSTB2024NSCQ-MSX1116), Open Research Fund of the State Key Laboratory of Brain-Machine Intelligence, Zhejiang University (BMI2500002).

Author contributions

J.W, K.C, B.C and X.D contributed to the conception and design of the study. J.C, Y.L, W.L, M.C and Y.W contributed to the acquisition and analysis of data; P.X, X.T, and T.Z, contributed to material preparation and data collection; J.C, Y.L, B.C, K.C and J.W wrote and edited the manuscript. All the authors discussed the paper.

Conflict of Interest

The authors declare no competing interests.

Reference

1 Payne, J. L. & Maguire, J. Pathophysiological mechanisms implicated in postpartum depression. *Frontiers in neuroendocrinology* **52**, 165-180 (2019). https://doi.org/10.1016/j.yfrne.2018.12.001

2 Falah-Hassani, K., Shiri, R. & Dennis, C. L. Prevalence and risk factors for comorbid postpartum depressive symptomatology and anxiety. *Journal of affective disorders* **198**, 142-147 (2016). https://doi.org/10.1016/j.jad.2016.03.010

3 Batt, M. M., Duffy, K. A., Novick, A. M., Metcalf, C. A. & Epperson, C. N. Is Postpartum Depression Different From Depression Occurring Outside of the Perinatal Period? A Review of the Evidence. *Focus (Am Psychiatr Publ)* **18**, 106-119 (2020). https://doi.org/10.1176/appi.focus.20190045

4 Pearlstein, T., Howard, M., Salisbury, A. & Zlotnick, C. Postpartum depression. *Am J Obstet Gynecol* **200**, 357-364 (2009). https://doi.org/10.1016/j.ajog.2008.11.033

5 Cheng, B. *et al.* Postpartum depression and major depressive disorder: the same or not? Evidence from resting-state functional MRI. *Psychoradiology* **2**, 121-128 (2022). https://doi.org/10.1093/psyrad/kkac015

6 Wisner, K. L., Moses-Kolko, E. L. & Sit, D. K. Postpartum depression: a disorder in search of a definition. *Arch Womens Ment Health* **13**, 37-40 (2010). https://doi.org/10.1007/s00737-009-0119-9

7 Farr, S. L., Dietz, P. M., O'Hara, M. W., Burley, K. & Ko, J. Y. Postpartum anxiety and comorbid depression in a population-based sample of women. *Journal of women's health (2002)* **23**, 120-128 (2014). https://doi.org/10.1089/jwh.2013.4438

8 Goodman, J. H. Paternal postpartum depression, its relationship to maternal postpartum depression, and implications for family health. *Journal of advanced nursing* **45**, 26-35 (2004). https://doi.org/10.1046/j.1365-2648.2003.02857.x

9 Hendrick, V., Altshuler, L., Strouse, T. & Grosser, S. Postpartum and nonpostpartum depression: differences in presentation and response to pharmacologic treatment. *Depression and anxiety* **11**, 66-72 (2000). https://doi.org/10.1002/(sici)1520-6394(2000)11:2<66::aid-da3>3.0.co;2-d

10 Cheng, B. *et al.* Abnormal dynamics of resting-state functional activity and couplings in postpartum depression with and without anxiety. *Cereb Cortex* **32**, 5597-5608 (2022). https://doi.org/10.1093/cercor/bhac038

11 Cheng, B. *et al.* Social support mediates the influence of cerebellum functional connectivity strength on postpartum depression and postpartum depression with anxiety. *Transl Psychiatry* **12**, 54 (2022). https://doi.org/10.1038/s41398-022-01781-9

12 Cheng, B. *et al.* Altered functional connectivity density and couplings in postpartum depression with and without anxiety. *Soc Cogn Affect Neurosci* **17**, 756-766 (2022). https://doi.org/10.1093/scan/nsab127

13 Brucar, L. R., Feczko, E., Fair, D. A. & Zilverstand, A. Current Approaches in Computational Psychiatry for the Data-Driven Identification of Brain-Based Subtypes. *Biol Psychiatry* **93**, 704-716 (2023).

https://doi.org/10.1016/j.biopsych.2022.12.020

14 Drysdale, A. T. *et al.* Resting-state connectivity biomarkers define neurophysiological subtypes of depression. *Nature medicine* **23**, 28-38 (2017). https://doi.org/10.1038/nm.4246

15 Chen, J. *et al.* Neural–genetic–environmental evidence for a disease factor in mental and physical health multimorbidity. *Nature Communications* **16**, 10088 (2025).

16 Wen J, V. E., Yang Z, et al. . Subtyping Brain Diseases from Imaging Data. *In: Colliot O, editor. Machine Learning for Brain Disorders [Internet]. New York, NY: Humana; 2023. Chapter 16. Available from: https://www.ncbi.nlm.nih.gov/books/NBK597476/ doi: 10.1007/978-1-0716-3195-9_16* (2023 Jul 23).

17 Wang, H., Jin, X., Zhang, Y. & Wang, J. Single-subject morphological brain networks: connectivity mapping, topological characterization and test–retest reliability. *Brain and Behavior* **6**, e00448 (2016). https://doi.org/https://doi.org/10.1002/brb3.448

18 Sun, H. *et al.* Mapping individual structural covariance network in development brain with dynamic time warping. *Cerebral Cortex* **34**, bhae039 (2024). https://doi.org/10.1093/cercor/bhae039

19 Kassem, M. S. *et al.* Stress-Induced Grey Matter Loss Determined by MRI Is Primarily Due to Loss of Dendrites and Their Synapses. *Molecular Neurobiology* **47**, 645-661 (2013). https://doi.org/10.1007/s12035-012-8365-7

20 Gogtay, N. & Thompson, P. M. Mapping gray matter development: implications for typical development and vulnerability to psychopathology. *Brain Cogn* **72**, 6-15 (2010). https://doi.org/10.1016/j.bandc.2009.08.009

21 Cheng, B. *et al.* Prolactin mediates the relationship between regional gray matter volume and postpartum depression symptoms. *Journal of affective disorders* **301**, 253-259 (2022). https://doi.org/https://doi.org/10.1016/j.jad.2022.01.051

22 Alexander-Bloch, A., Giedd, J. N. & Bullmore, E. Imaging structural co-variance between human brain regions. *Nature reviews. Neuroscience* **14**, 322-336 (2013). https://doi.org/10.1038/nrn3465

23 Mechelli, A., Friston, K. J., Frackowiak, R. S. & Price, C. J. Structural covariance in the human cortex. *The Journal of neuroscience : the official journal of the Society for Neuroscience* **25**, 8303-8310 (2005). https://doi.org/10.1523/jneurosci.0357-05.2005

24 Zielinski, B. A., Gennatas, E. D., Zhou, J. & Seeley, W. W. Network-level structural covariance in the developing brain. *Proceedings of the National Academy of Sciences of the United States of America* **107**, 18191-18196 (2010). https://doi.org/10.1073/pnas.1003109107

25 Montembeault, M. *et al.* The impact of aging on gray matter structural covariance networks. *NeuroImage* **63**, 754-759 (2012). https://doi.org/10.1016/j.neuroimage.2012.06.052

26 Zhang, S. *et al.* Using individualized structural covariance networks to analyze the heterogeneity of cerebral small vessel disease with cognitive impairment. *Journal of Stroke and Cerebrovascular Diseases*

33, 107829 (2024). https://doi.org/https://doi.org/10.1016/j.jstrokecerebrovasdis.2024.107829

27 Han, S. *et al.* Resolving heterogeneity in depression using individualized structural covariance network analysis. *Psychological medicine* **53**, 5312-5321 (2023). https://doi.org/10.1017/s0033291722002380

28 Liu, Z. *et al.* Resolving heterogeneity in schizophrenia through a novel systems approach to brain structure: individualized structural covariance network analysis. *Mol Psychiatry* **26**, 7719-7731 (2021). https://doi.org/10.1038/s41380-021-01229-4

29 Zhang, H. *et al.* Reorganization of cortical individualized differential structural covariance network is associated with regional morphometric changes in chronic subcortical stroke. *NeuroImage. Clinical* **45**, 103735 (2025). https://doi.org/10.1016/j.nicl.2025.103735

30 Li, W. *et al.* Disentangling the Switching Behavior in Functional Connectivity Dynamics in Autism Spectrum Disorder: Insights from Developmental Cohort Analysis and Molecular-Cellular Associations. *Adv Sci (Weinh)* **12**, e2403801 (2025). https://doi.org/10.1002/advs.202403801

31 Cox, J. L., Holden, J. M. & Sagovsky, R. Detection of postnatal depression. Development of the 10-item Edinburgh Postnatal Depression Scale. *Br J Psychiatry* **150**, 782-786 (1987). https://doi.org/10.1192/bjp.150.6.782

32 Beck, A. T., Ward, C. H., Mendelson, M., Mock, J. & Erbaugh, J. An inventory for measuring depression. *Arch Gen Psychiatry* **4**, 561-571 (1961). https://doi.org/10.1001/archpsyc.1961.01710120031004

33 Beck, A. T., Epstein, N., Brown, G. & Steer, R. A. An inventory for measuring clinical anxiety: psychometric properties. *J Consult Clin Psychol* **56**, 893-897 (1988). https://doi.org/10.1037//0022-006x.56.6.893

34 Buysse, D. J., Reynolds, C. F., 3rd, Monk, T. H., Berman, S. R. & Kupfer, D. J. The Pittsburgh Sleep Quality Index: a new instrument for psychiatric practice and research. *Psychiatry Res* **28**, 193-213 (1989). https://doi.org/10.1016/0165-1781(89)90047-4

35 Logsdon, M. C. & Usui, W. M. The Postpartum Support Questionnaire: psychometric properties in adolescents. *J Child Adolesc Psychiatr Nurs* **19**, 145-156 (2006). https://doi.org/10.1111/j.1744-6171.2006.00062.x

36 Cohen, S. & Williamson, G. M. Perceived Stress in a Probability Sample of the United-States. *Clar Symp*, 31-67 (1988).

37 Ashburner, J. A fast diffeomorphic image registration algorithm. *Neuroimage* **38**, 95-113 (2007). https://doi.org/10.1016/j.neuroimage.2007.07.007

38 Margulies, D. S. *et al.* Situating the default-mode network along a principal gradient of macroscale cortical organization. *Proc Natl Acad Sci U S A* **113**, 12574-12579 (2016). https://doi.org/10.1073/pnas.1608282113

39 Liu, Z. W. *et al.* Resolving heterogeneity in schizophrenia through a novel systems approach to brain

structure: individualized structural covariance network analysis. *Mol Psychiatr* **26**, 7719-7731 (2021). https://doi.org/10.1038/s41380-021-01229-4

40 Hawrylycz, M. J. *et al.* An anatomically comprehensive atlas of the adult human brain transcriptome. *Nature* **489**, 391-399 (2012). https://doi.org/10.1038/nature11405

41 Markello, R. D. *et al.* Standardizing workflows in imaging transcriptomics with the abagen toolbox. *Elife* **10** (2021). https://doi.org/10.7554/eLife.72129

42 Arnatkeviciute, A., Fulcher, B. D. & Fornito, A. A practical guide to linking brain-wide gene expression and neuroimaging data. *Neuroimage* **189**, 353-367 (2019). https://doi.org/10.1016/j.neuroimage.2019.01.011

43 Schaefer, A. *et al.* Local-Global Parcellation of the Human Cerebral Cortex from Intrinsic Functional Connectivity MRI. *Cereb Cortex* **28**, 3095-3114 (2018). https://doi.org/10.1093/cercor/bhx179

44 Hansen, J. Y. *et al.* Mapping neurotransmitter systems to the structural and functional organization of the human neocortex. *Nat Neurosci* **25**, 1569-1581 (2022). https://doi.org/10.1038/s41593-022-01186-3

45 Bauer, A. E. *et al.* Identification and validation of postpartum depression subtypes: a population-based cohort study. *EClinicalMedicine* **89**, 103540 (2025). https://doi.org/10.1016/j.eclinm.2025.103540

46 Chen, K. *et al.* Shared and disorder-specific large-scale intrinsic and effective functional network connectivities in postpartum depression with and without anxiety. *Cereb Cortex* **34** (2024). https://doi.org/10.1093/cercor/bhae478

47 Chen, K. x. *et al.* Molecular basis underlying default mode network functional abnormalities in postpartum depression with and without anxiety. *Hum Brain Mapp* **45**, e26657 (2024).

48 Batty, M. J. *et al.* Cortical gray matter in attention-deficit/hyperactivity disorder: a structural magnetic resonance imaging study. *J Am Acad Child Adolesc Psychiatry* **49**, 229-238 (2010). https://doi.org/10.1016/j.jaac.2009.11.008

49 Cafiero, P. J. & Justich Zabala, P. Postpartum depression: Impact on pregnant women and the postnatal physical, emotional, and cognitive development of their children. An ecological perspective. *Arch Argent Pediatr* **122**, e202310217 (2024). https://doi.org/10.5546/aap.2023-10217.eng

50 Qiu, T., Wen, H., Liu, Z. X., Pan, X. P. & Zeng, T. Investigation Regarding Early Cognitive Function of Women in the Postpartum Period and the Analysis of Influencing Factors. *Risk Manag Healthc Policy* **14**, 3747-3754 (2021). https://doi.org/10.2147/RMHP.S309553

51 Ives-Deliperi, V. & Butler, J. T. Mechanisms of cognitive impairment in temporal lobe epilepsy: A systematic review of resting-state functional connectivity studies. *Epilepsy Behav* **115**, 107686 (2021). https://doi.org/10.1016/j.yebeh.2020.107686

52 Huang, S., Li, M., Huang, C. & Liu, J. Acute limbic system connectivity predicts chronic cognitive function in mild traumatic brain injury: An individualized differential structural covariance network

study. *Pharmacol Res* **206**, 107274 (2024). https://doi.org/10.1016/j.phrs.2024.107274

53 Liu, Y. *et al.* Transcriptional patterns of amygdala functional connectivity in first-episode, drug-naive major depressive disorder. *Transl Psychiatry* **14**, 351 (2024). https://doi.org/10.1038/s41398-024-03062-z

54 Ramasubbu, R. *et al.* Reduced intrinsic connectivity of amygdala in adults with major depressive disorder. *Front Psychiatry* **5**, 17 (2014). https://doi.org/10.3389/fpsyt.2014.00017

55 Sun, H. *et al.* Functional connectivity analyses of individual hippocampal subregions in major depressive disorder with electroconvulsive therapy. *Psychoradiology* **4**, kkae030 (2024). https://doi.org/10.1093/psyrad/kkae030

56 Moreira, L. K. S. *et al.* Post-partum depression: From clinical understanding to preclinical assessments. *Front Psychiatry* **14**, 1173635 (2023). https://doi.org/10.3389/fpsyt.2023.1173635

57 Okun, M. L. Disturbed Sleep and Postpartum Depression. *Curr Psychiatry Rep* **18**, 66 (2016). https://doi.org/10.1007/s11920-016-0705-2

58 Tabaeifard, R. *et al.* Association between oxidative balance score and risk of postpartum depression in Iranian women: a prospective cohort study. *Sci Rep* **15**, 8590 (2025). https://doi.org/10.1038/s41598-025-93206-y

59 Gorman-Sandler, E. *et al.* Mitochondrial might: powering the peripartum for risk and resilience. *Front Behav Neurosci* **17**, 1286811 (2023). https://doi.org/10.3389/fnbeh.2023.1286811

60 McEwen, A. M. *et al.* Increased glutamate levels in the medial prefrontal cortex in patients with postpartum depression. *Neuropsychopharmacology* **37**, 2428-2435 (2012). https://doi.org/10.1038/npp.2012.101

61 Ghuman, A. *et al.* Prospective Investigation of Glutamate Levels and Percentage Gray Matter in the Medial Prefrontal Cortex in Females at Risk for Postpartum Depression. *Curr Neuropharmacol* **20**, 1988-2000 (2022). https://doi.org/10.2174/1570159x20666220302101115

62 Quoidbach, J., Mikolajczak, M. & Gross, J. J. Positive interventions: An emotion regulation perspective. *Psychol Bull* **141**, 655-693 (2015). https://doi.org/10.1037/a0038648

63 Cheng, B. *et al.* Altered functional connectivity density and couplings in postpartum depression with and without anxiety. *Social cognitive and affective neuroscience* **17**, 756-766 (2022). https://doi.org/10.1093/scan/nsab127

64 Brown, J. V. E. *et al.* Antidepressant treatment for postnatal depression. *Cochrane Database of Systematic Reviews* (2021).

65 Raichle, M. E. The brain's default mode network. *Annu Rev Neurosci* **38**, 433-447 (2015). https://doi.org/10.1146/annurev-neuro-071013-014030

66 Raichle, M. E. *et al.* A default mode of brain function. *Proceedings of the National Academy of Sciences of the United States of America* **98**, 676-682 (2001). https://doi.org/10.1073/pnas.98.2.676

67 Chase, H. W., Moses-Kolko, E. L., Zevallos, C., Wisner, K. L. & Phillips, M. L. Disrupted posterior cingulate–amygdala connectivity in postpartum depressed women as measured with resting BOLD fMRI. *Social Cognitive and Affective Neuroscience* **9**, 1069-1075 (2014). https://doi.org/10.1093/scan/nst083

68 Li, W. *et al.* Disentangling the Switching Behavior in Functional Connectivity Dynamics in Autism Spectrum Disorder: Insights from Developmental Cohort Analysis and Molecular-Cellular Associations. *Advanced Science* **n/a**, 2403801 (2025). https://doi.org/https://doi.org/10.1002/advs.202403801

69 Duan, C., Cosgrove, J. & Deligiannidis, K. M. Understanding Peripartum Depression Through Neuroimaging: a Review of Structural and Functional Connectivity and Molecular Imaging Research. *Curr Psychiatry Rep* **19**, 70 (2017). https://doi.org/10.1007/s11920-017-0824-4

70 Kim, P. *et al.* The plasticity of human maternal brain: longitudinal changes in brain anatomy during the early postpartum period. *Behav Neurosci* **124**, 695-700 (2010). https://doi.org/10.1037/a0020884

71 Wang, J. *et al.* The critical mediating roles of the middle temporal gyrus and ventrolateral prefrontal cortex in the dynamic processing of interpersonal emotion regulation. *Neuroimage* **300**, 120789 (2024). https://doi.org/10.1016/j.neuroimage.2024.120789

72 Šimić, G. *et al.* Understanding Emotions: Origins and Roles of the Amygdala. *Biomolecules* **11** (2021). https://doi.org/10.3390/biom11060823

73 Zhu, Y. *et al.* Emotion Regulation of Hippocampus Using Real-Time fMRI Neurofeedback in Healthy Human. *Front Hum Neurosci* **13**, 242 (2019). https://doi.org/10.3389/fnhum.2019.00242

74 Landi, N. *et al.* Maternal neural responses to infant cries and faces: relationships with substance use. *Front Psychiatry* **2**, 32 (2011). https://doi.org/10.3389/fpsyt.2011.00032

75 Chen, G. *et al.* Environmental enrichment attenuates depressive-like behavior in maternal rats by inhibiting neuroinflammation and apoptosis and promoting neuroplasticity. *Neurobiol Stress* **30**, 100624 (2024). https://doi.org/10.1016/j.ynstr.2024.100624

76 Post, C. & Leuner, B. The maternal reward system in postpartum depression. *Arch Womens Ment Health* **22**, 417-429 (2019). https://doi.org/10.1007/s00737-018-0926-y

77 Jacob, Y. *et al.* Neural correlates of rumination in major depressive disorder: A brain network analysis. *Neuroimage Clin* **25**, 102142 (2020). https://doi.org/10.1016/j.nicl.2019.102142

78 Benarroch, E. E. Synaptic effects of cannabinoids: complexity, behavioral effects, and potential clinical implications. *Neurology* **83**, 1958-1967 (2014). https://doi.org/10.1212/WNL.0000000000001013

79 Ribeiro, S. C., Kennedy, S. E., Smith, Y. R., Stohler, C. S. & Zubieta, J. K. Interface of physical and emotional stress regulation through the endogenous opioid system and mu-opioid receptors. *Prog Neuropsychopharmacol Biol Psychiatry* **29**, 1264-1280 (2005). https://doi.org/10.1016/j.pnpbp.2005.08.011

80 Delgado, P. L. Depression: the case for a monoamine deficiency. *J Clin Psychiatry* **61 Suppl 6**, 7-11

(2000).

81 Della Corte, L. *et al.* Prevalence and associated psychological risk factors of postpartum depression: a cross-sectional study. *J Obstet Gynaecol* **42**, 976-980 (2022). https://doi.org/10.1080/01443615.2021.1980512

82 Hopkins, J., Marcus, M. & Campbell, S. B. Postpartum depression: a critical review. *Psychol Bull* **95**, 498-515 (1984).

83 Costa-Brito, A. R., Goncalves, I. & Santos, C. R. A. The brain as a source and a target of prolactin in mammals. *Neural Regen Res* **17**, 1695-1702 (2022). https://doi.org/10.4103/1673-5374.332124

84 Xu, Y. *et al.* The Association Between Prolactin Levels and Cognitive Function in Female Patients With Severe Mental Disorders. *Psychiatry Investig* **21**, 832-837 (2024). https://doi.org/10.30773/pi.2024.0008

Figure Legend

Figure 1. Definition of PPD Subtypes and Associated Structural Abnormalities. (a) Silhouette coefficients across different numbers of clusters. (b) Brain regions showing significant GMV differences between Subtype 1 (n = 44) and healthy postpartum women (HPW) (n = 62), identified using two-sample t-tests with Gaussian Random Field (GRF) correction ($p < 0.05$). The distribution of these regions across the seven canonical brain networks is shown on the right, along with their functional annotations derived from Neurosynth. (c) Brain regions showing significantly increased GMV in Subtype 2 (n = 32) compared with HPW (n = 62), identified and annotated following the same procedure. (d) Brain regions showing significantly lower GMV in Subtype 1 (n = 44) compared with Subtype 2 (n = 32), identified and annotated similarly. (e) Whole-brain voxel-wise maps of correlations between GMV and clinical measures (BDI, EPDS) as well as hormonal levels (estradiol, progesterone, and prolactin) in separately Subtype 1 (n = 44) and Subtype 2 (n = 32). (f) Correlation heatmaps showing the associations between the mean GMV of the significant regions identified in panels b–d and clinical as well as hormonal measures. Red boxes indicate correlations with $p < 0.05$ (uncorrected). DOR, dorsal attention network; SOM, somatosensory motor network; DMN, default mode network; VEN, ventral attention network; VIS, visual networks; LIM, limbic network; FPC, frontoparietal network.

Figure 2. Heterogeneity Analysis of Individual Differential Structural Covariance Connectivity for PPD Subtypes. (a) 26 edges showing significant deviations in at least 10% of PPD patients (≥ 8 cases) are presented. (b) z-score distributions of these 26 connections across the two subtypes. Blue and red curves represent the mean z-scores for Subtype 1 (n = 44) and Subtype 2 (n = 32), respectively. Shaded areas indicate the standard error of the mean (SEM). (c) Two edges demonstrating significant intergroup differences (two-sided Welch's t-test, FDR-corrected, $p_{adj} < 0.05$), with right panel showing their anatomical representations.

Figure 3. Association between Brain Structural Changes of PPD Subtypes and Transcriptomic Profiles. (a) Spatial distribution of partial least squares (PLS1) scores in the left hemisphere for Subtype 1 (left top), along with spatial correlations between PLS1 scores and regional t-values (Subtype 1 vs. HPW, two-sided test) (left bottom). The shaded error bands represent the 95% confidence interval of the smoothed fit. The right panel displays the top 5 significantly enriched biological processes (BP) and molecular functions (MF) pathways for PLS1-associated genes (FDR-corrected, $p_{adj} < 0.05$). (b) Spatial distribution of PLS1 scores in the left hemisphere for Subtype 2 (left top), along with spatial correlations between PLS1 scores and regional t-values (Subtype 2 vs. HPW, two-sided test) (left bottom). The shaded error bands represent the 95% confidence interval of the smoothed fit. The right panel shows the top 5 significantly enriched BP and MF pathways for PLS1-associated genes (FDR-corrected, $p_{adj} < 0.05$).

Figure 4. Differential Neurotransmitter Contributions to Brain Structural Changes of PPD Subtypes. Multivariate linear regression models (two-sided) were employed to assess associations between neurotransmitter

systems and regional t-value maps (PPD subtypes vs. HPW, two-sided Welch's t-test). Neurotransmitter systems marked with green boxes remained statistically significant after FDR-correction (p_{adj} (q) < 0.05).

ED Summary:

Chen et al. apply unsupervised clustering to structural brain images of women with postpartum depression and integrate molecular data to characterize neurobiological variation. The study identifies two distinct subtypes with different structural, connectivity, and molecular profiles that may guide personalized care.

Peer review information: *Communications Medicine* thanks Yasmin Harrington, Xiaoyu Tong and the other, anonymous, reviewer(s) for their contribution to the peer review of this work. A peer review file is available.

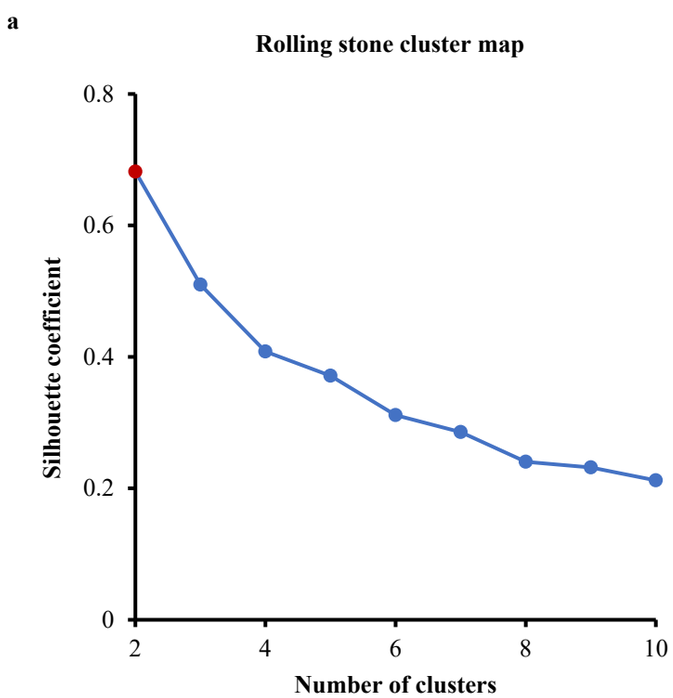
a
Rolling stone cluster map
Silhouette coefficient
0.8
0.6
0.4
0.2
0
2
4
6
8
10
Number of clusters

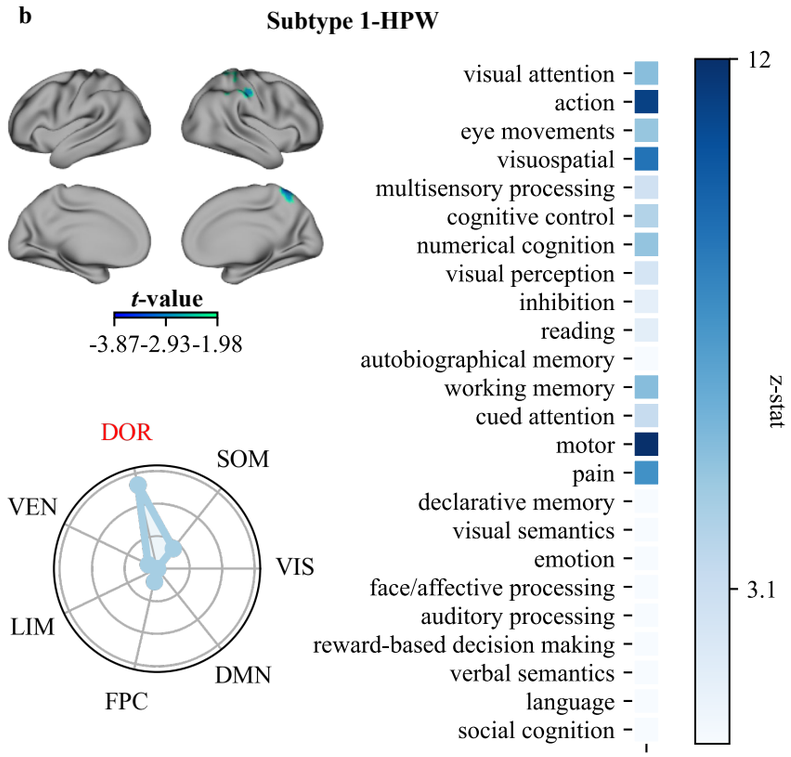
b
Subtype 1-HPW
t-value
-3.87-2.93-1.98
DOR
SOM
VIS
DMN
FPC
LIM
VEN
visual attention
action
eye movements
visuospatial
multisensory processing
cognitive control
numerical cognition
visual perception
inhibition
reading
autobiographical memory
working memory
cued attention
motor
pain
declarative memory
visual semantics
emotion
face/affective processing
auditory processing
reward-based decision making
verbal semantics
language
social cognition
12
z-stat
3.1
0-5

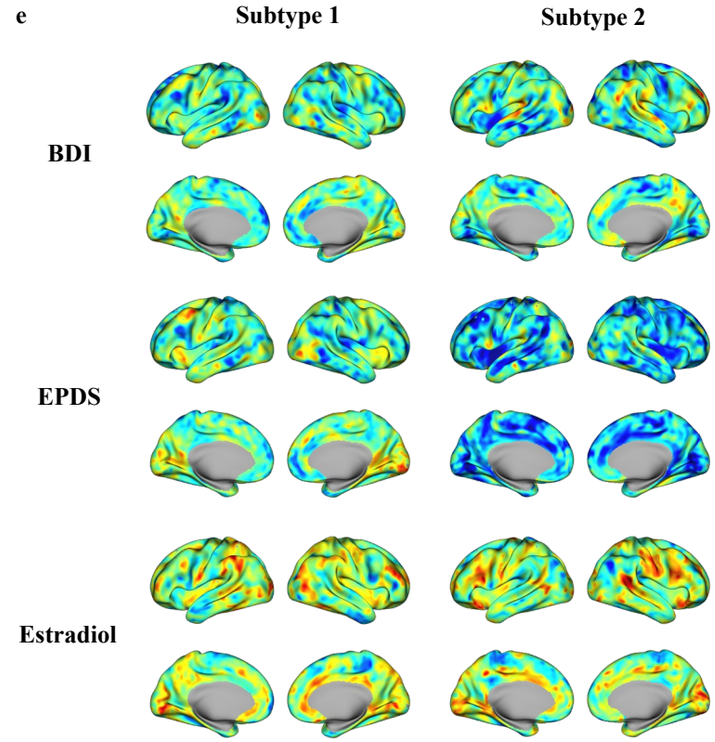
e
Subtype 1
Subtype 2
BDI
EPDS
Estradiol
Progesterone
Prolactin
r
-0.60
0.60

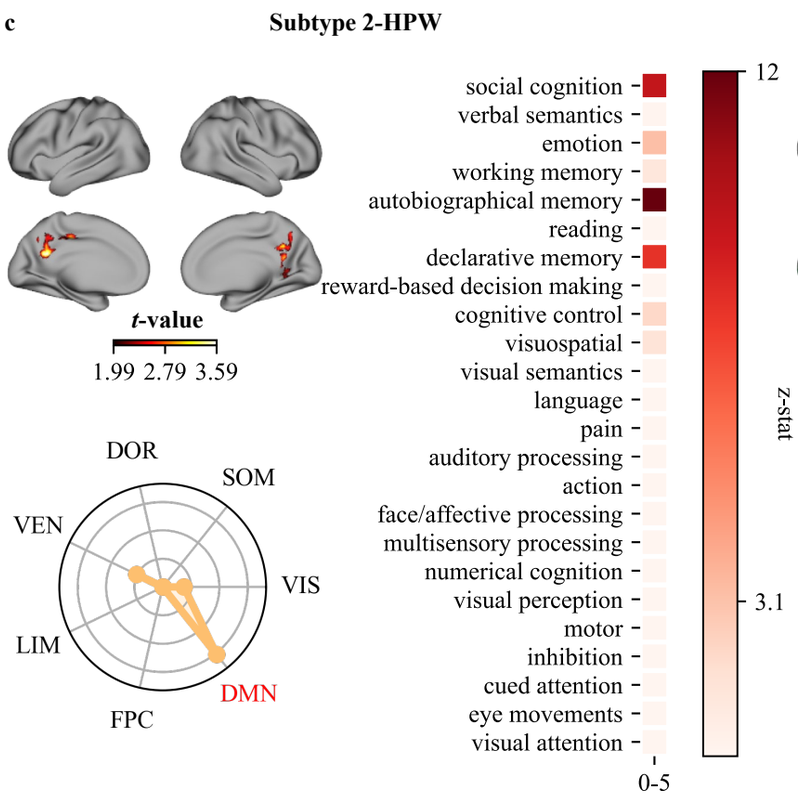
c
Subtype 2-HPW
t-value
1.99 2.79 3.59
DOR
SOM
VIS
DMN
FPC
LIM
VEN
social cognition
verbal semantics
emotion
working memory
autobiographical memory
reading
declarative memory
reward-based decision making
cognitive control
visuospatial
visual semantics
language
pain
auditory processing
action
face/affective processing
multisensory processing
numerical cognition
visual perception
motor
inhibition
cued attention
eye movements
visual attention
12
z-stat
3.1
0-5

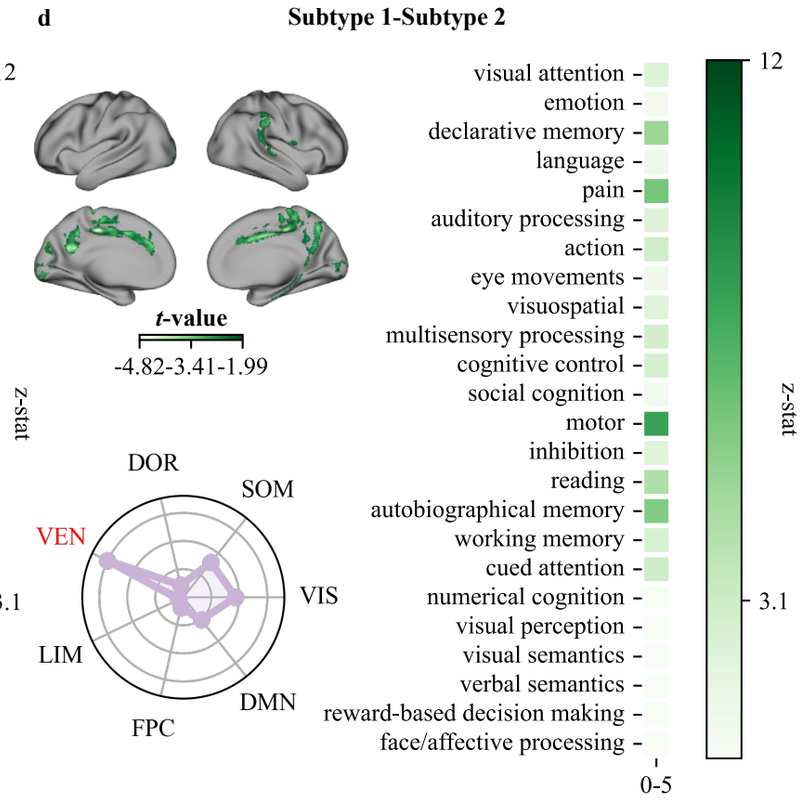
d
Subtype 1-Subtype 2
t-value
-4.82-3.41-1.99
DOR
SOM
VIS
DMN
FPC
LIM
VEN
visual attention
emotion
declarative memory
language
pain
auditory processing
action
eye movements
visuospatial
multisensory processing
cognitive control
social cognition
motor
inhibition
reading
autobiographical memory
working memory
cued attention
numerical cognition
visual perception
visual semantics
verbal semantics
reward-based decision making
face/affective processing
12
z-stat
3.1
0-5

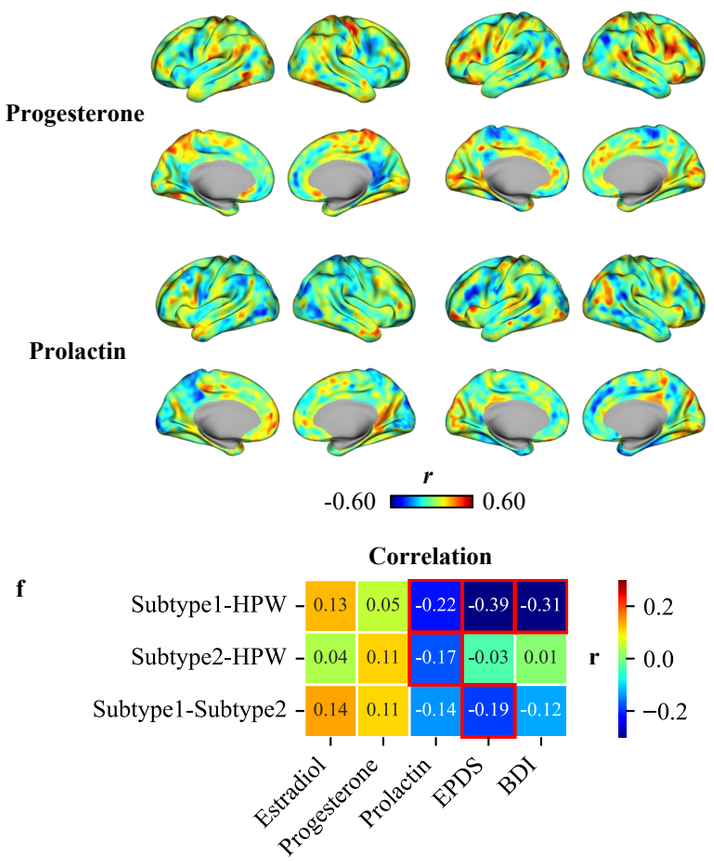
Progesterone
Prolactin
r
-0.60
0.60
f
Correlation
Subtype1-HPW
Subtype2-HPW
Subtype1-Subtype2
0.13
0.05
-0.22
-0.39
-0.31
0.04
0.11
-0.17
-0.03
0.01
0.14
0.11
-0.14
-0.19
-0.12
r
0.2
0.0
−0.2
Estradiol
Progesterone
Prolactin
EPDS
BDI

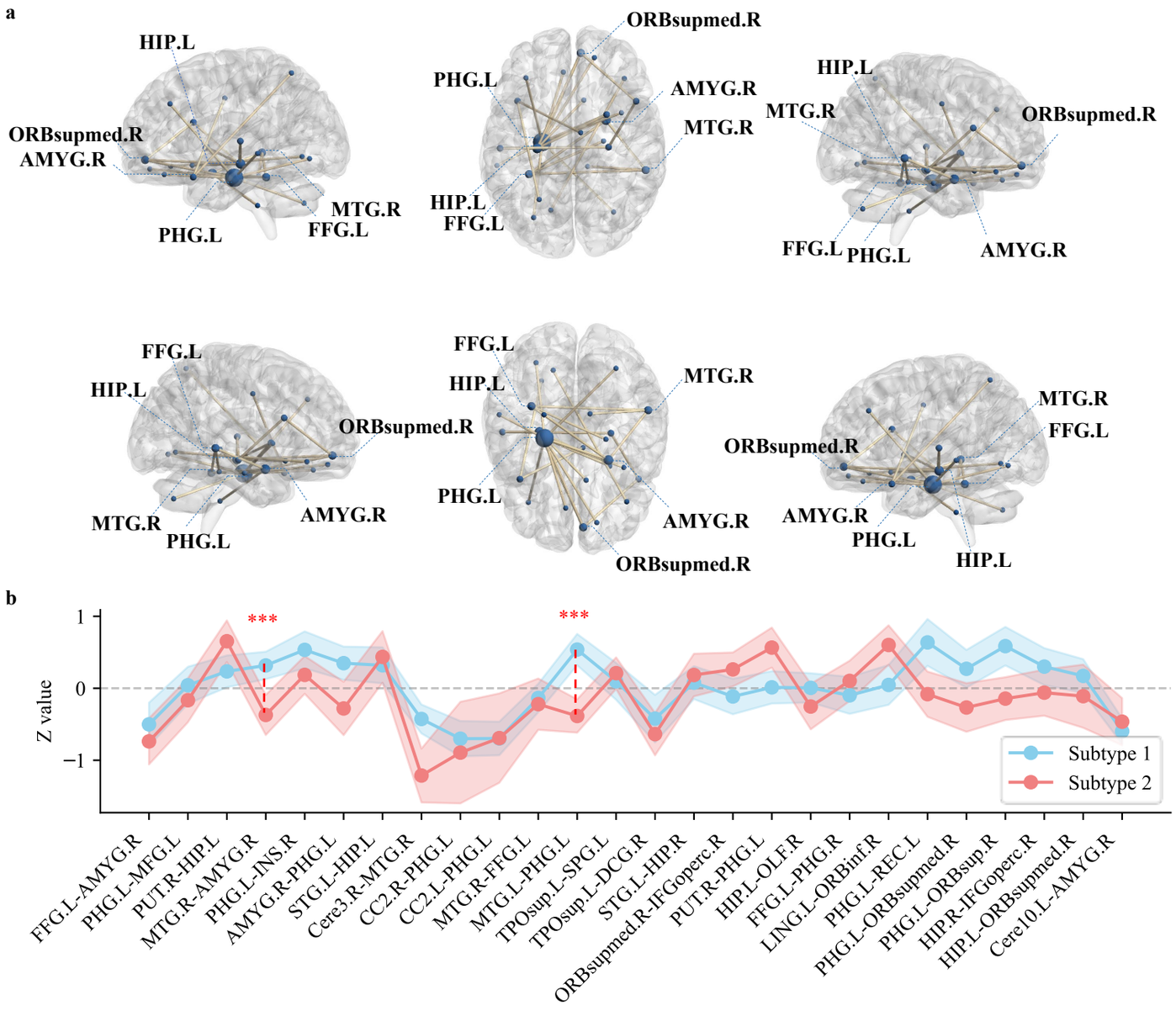
a
HIP.L
ORBsupmed.R
AMYG.R
MTG.R
FFG.L
PHG.L
ORBsupmed.R
PHG.L
AMYG.R
MTG.R
HIP.L
FFG.L
HIP.L
MTG.R
ORBsupmed.R
FFG.L
PHG.L
AMYG.R
FFG.L
HIP.L
ORBsupmed.R
MTG.R
PHG.L
AMYG.R
FFG.L
HIP.L
MTG.R
PHG.L
AMYG.R
ORBsupmed.R
MTG.R
FFG.L
ORBsupmed.R
AMYG.R
PHG.L
HIP.L
b
***
***
Z value
1
0
−1
Subtype 1
Subtype 2
FFG.L-AMYG.R
PHG.L-MFG.L
PUT.R-HIP.L
MTG.R-AMYG.R
PHG.L-INS.R
AMYG.R-PHG.L
STG.L-HIP.L
Cere3.R-MTG.R
CC2.R-PHG.L
CC2.L-PHG.L
MTG.R-FFG.L
MTG.L-PHG.L
TPOsup.L-SPG.L
TPOsup.L-DCG.R
ORBsupmed.R-IFGoperc.R
STG.L-HIP.R
PUT.R-PHG.L
HIP.L-OLF.R
FFG.L-PHG.R
LING.L-ORBinf.R
PHG.L-REC.L
PHG.L-ORBsupmed.R
PHG.L-ORBsup.R
HIP.R-IFGoperc.R
HIP.L-ORBsupmed.R
Cere10.L-AMYG.R
c
Z value
5.0
2.5
0.0
−2.5
−5.0
MTG.L-PHG.L
MTG.R-AMYG.R
Subtype 1
Subtype 2
L
R
L
R
Mean z value
-0.5
0.0
0.5

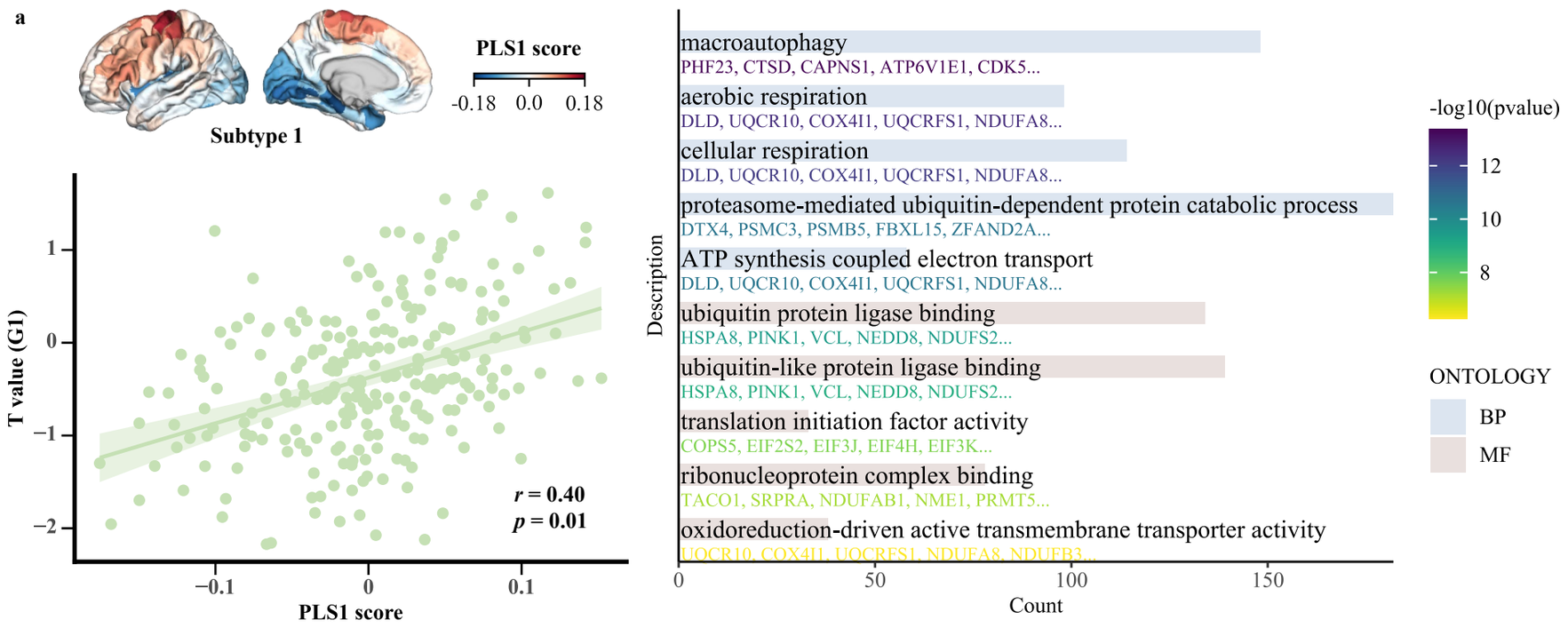
a
PLS1 score
-0.18 0.0 0.18
Subtype 1
T value (G1)
PLS1 score
r = 0.40
p = 0.01
Description
macroautophagy
PHF23, CTSD, CAPNS1, ATP6V1E1, CDK5...
aerobic respiration
DLD, UQCR10, COX4I1, UQCRFS1, NDUFA8...
cellular respiration
DLD, UQCR10, COX4I1, UQCRFS1, NDUFA8...
proteasome-mediated ubiquitin-dependent protein catabolic process
DTX4, PSMC3, PSMB5, FBXL15, ZFAND2A...
ATP synthesis coupled electron transport
DLD, UQCR10, COX4I1, UQCRFS1, NDUFA8...
ubiquitin protein ligase binding
HSPA8, PINK1, VCL, NEDD8, NDUFS2...
ubiquitin-like protein ligase binding
HSPA8, PINK1, VCL, NEDD8, NDUFS2...
translation initiation factor activity
COPS5, EIF2S2, EIF3J, EIF4H, EIF3K...
ribonucleoprotein complex binding
TACO1, SRPRA, NDUFAB1, NME1, PRMT5...
oxidoreduction-driven active transmembrane transporter activity
UQCR10, COX4I1, UQCRFS1, NDUFA8, NDUFB3...
Count
-log10(pvalue)
ONTOLOGY
BP
MF

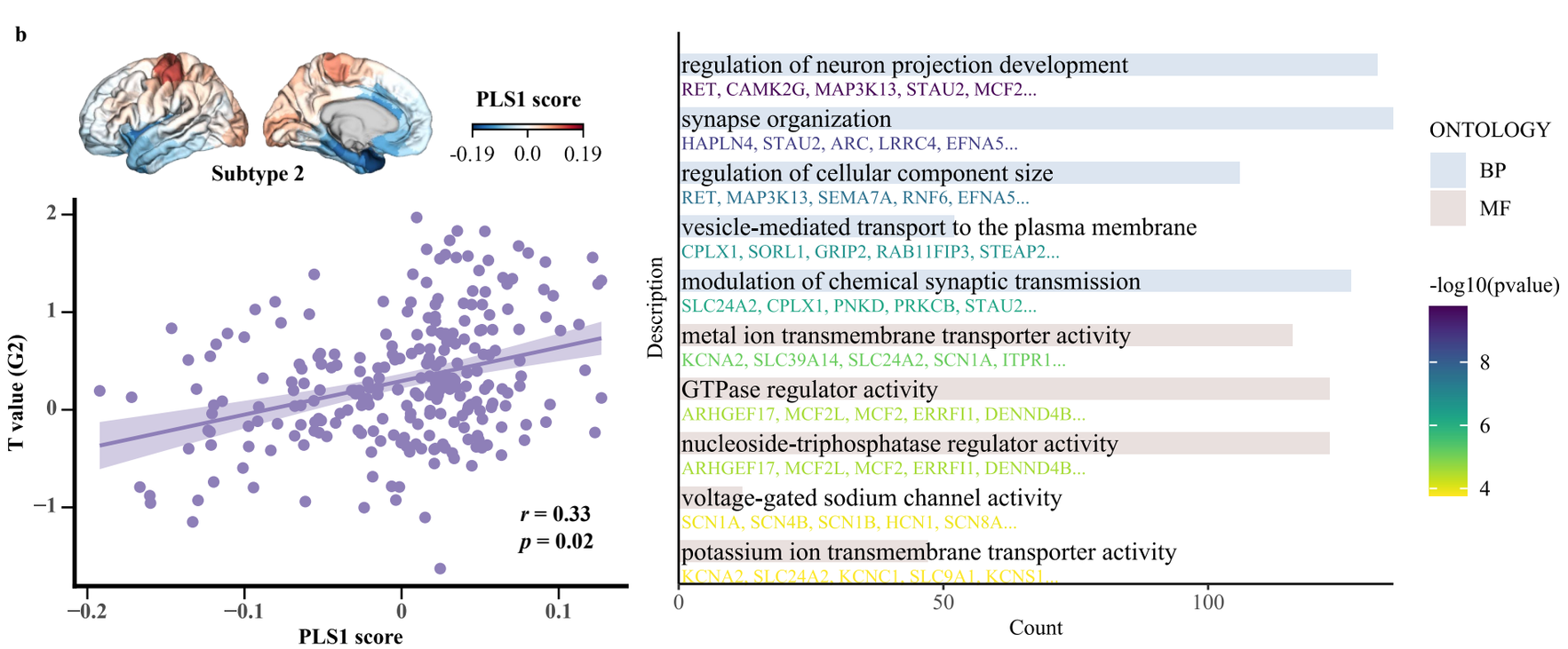
b
PLS1 score
-0.19 0.0 0.19
Subtype 2
T value (G2)
PLS1 score
r = 0.33
p = 0.02
Description
regulation of neuron projection development
RET, CAMK2G, MAP3K13, STAU2, MCF2...
synapse organization
HAPLN4, STAU2, ARC, LRRC4, EFNA5...
regulation of cellular component size
RET, MAP3K13, SEMA7A, RNF6, EFNA5...
vesicle-mediated transport to the plasma membrane
CPLX1, SORL1, GRIP2, RAB11FIP3, STEAP2...
modulation of chemical synaptic transmission
SLC24A2, CPLX1, PNKD, PRKCB, STAU2...
metal ion transmembrane transporter activity
KCNA2, SLC39A14, SLC24A2, SCN1A, ITPR1...
GTPase regulator activity
ARHGEF17, MCF2L, MCF2, ERRFI1, DENND4B...
nucleoside-triphosphatase regulator activity
ARHGEF17, MCF2L, MCF2, ERRFI1, DENND4B...
voltage-gated sodium channel activity
SCN1A, SCN4B, SCN1B, HCN1, SCN8A...
potassium ion transmembrane transporter activity
KCNA2, SLC24A2, KCNC1, SLC9A1, KCNS1...
Count
ONTOLOGY
BP
MF
-log10(pvalue)

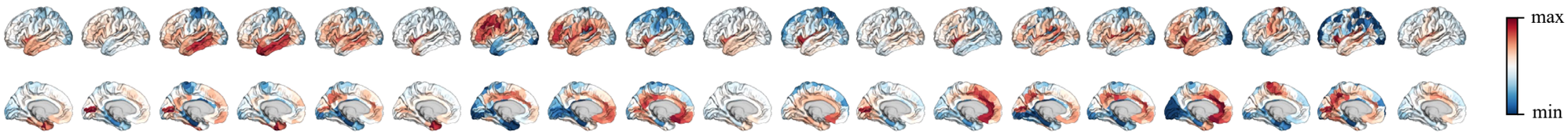

	5-HT$_{1A}$	5-HT$_{1B}$	5-HT$_{2A}$	5-HT$_4$	5-HT$_6$	5-HTT	$\alpha_4\beta_2$	CB$_1$	D$_1$	D$_2$	DAT	GABA$_{a/BZ}$	H$_3$	M$_1$	mGluR$_5$	MOR	NET	NMDA	VAChT
Subtype 1	-0.07 q = 0.67	-0.27 q = 0.22	0.35 q = 0.38	-0.17 q = 0.43	0.11 q = 0.62	-0.06 q = 0.67	0.09 q = 0.48	0.13 q = 0.51	-0.18 q = 0.41	-0.02 q = 0.89	-0.27 q = 0.22	0.24 q = 0.22	0.08 q = 0.53	-0.10 q = 0.56	-0.50 q = 0.00	0.28 q = 0.22	-0.00 q = 0.99	0.17 q = 0.38	0.16 q = 0.43
Subtype 2	-0.16 q = 0.29	-0.31 q = 0.03	0.25 q = 0.38	-0.12 q = 0.45	-0.20 q = 0.29	0.05 q = 0.66	-0.11 q = 0.29	-0.06 q = 0.66	-0.16 q = 0.29	-0.29 q = 0.03	-0.07 q = 0.66	0.11 q = 0.40	0.08 q = 0.40	0.31 q = 0.02	0.01 q = 0.92	0.32 q = 0.04	0.02 q = 0.92	0.18 q = 0.27	0.07 q = 0.66